

27 **Abstract**

28 Dust is an important aerosol affecting air quality in China in winter and spring
29 seasons. Dust in China is potentially influenced by the interannual climate variability
30 associated with El Niño. Here, the impacts of El Niño with different temporal and
31 spatial types on dust pollution in boreal winter and spring in China and the potential
32 mechanisms are investigated using a state-of-the-art earth system model (E3SMv1). We
33 find that the Eastern Pacific (EP) and Central Pacific (CP) El Niño both increase
34 wintertime dust concentrations by 5–50 $\mu\text{g m}^{-3}$ over central-eastern China. Due to a
35 stronger wind and lower relative humidity, which favor dust emissions near sources,
36 and a strengthened northwesterly and reduced precipitation, which are conducive to
37 dust transport, dust concentrations during the CP El Niño are 5–20 $\mu\text{g m}^{-3}$ higher in
38 northern China than during the EP El Niño, although the changes are mostly
39 insignificant. El Niño with a short duration (SD) increases boreal winter dust
40 concentrations by 20–100 $\mu\text{g m}^{-3}$ over northern China relative to the climatological
41 mean, while there is a decrease of 5–50 $\mu\text{g m}^{-3}$ during the long duration (LD) El Niño,
42 which are also related to the El Niño-induced changes in atmospheric circulation,
43 precipitation, and relative humidity. In the following spring season, all types of El Niño
44 events enhance dust over the northern China, but only the increase during the LD El
45 Niño is statistically significant, suggesting that the weaker intensity but longer duration
46 of the LD El Niño events can significantly affect spring dust in China. Our results
47 contribute the current knowledge of the influence of El Niño on dust pollution, which
48 have profound implications for air pollution control and dust storm prediction.

49 **1. Introduction**

50 Dust, one of the most important types of natural aerosols, has significant impacts
51 on Earth's radiative balance (Seinfeld et al., 2004), regional and global climate (Kok et
52 al, 2018; Yang et al.,2017), the hydrological cycle (Huang et al., 2014), agricultural
53 production (Sivakumar, 2005), public health and transportation activities (Goudie,
54 2014). The Gobi Desert and the Taklamakan Desert in northwestern China are
55 important contributors to dust concentrations in East Asia and even globally, and about
56 30% of the dust from the sources in China can be transported to the downwind areas
57 over long distances (Chen et al., 2017). Despite China's vigorous efforts to combat
58 desertification since the beginning of 21st century, strong and widespread dust storms
59 still occurred in China in recent years (Yin et al., 2021). Therefore, a deeper and more
60 scientific comprehension of the factors affecting dust aerosols in China is urgently
61 needed for the early warning and mitigation of dust pollution.

62 In recent years, the influence of meteorological conditions on dust pollution in
63 China has attracted considerable attention (Guo et al., 2019; Li et al., 2020; Lou et al.,
64 2016; Shi et al., 2021; Yin et al., 2021; Zhu et al., 2008). Under global warming in
65 recent decades, dust emissions and the frequency of dust storms in northern China
66 decreased (Shi et al., 2021), which was attributed to the reduced frequency and intensity
67 of Mongolian cyclones, related to the weakened westerly jet stream and atmospheric
68 pressure in northern China and Mongolia, in a warming climate (Zhu et al., 2008). Due
69 to a combination of changes in disruptive temperature anomalies in the Mongolian dust
70 source region, the occurrence of super Mongolian cyclone, and the anomalies of sea ice
71 in the Barents and Kara Sea and sea surface temperature (SST) in the east Pacific and
72 northwest Atlantic, China experienced the strongest dust pollution in spring 2021(Yin
73 et al., 2021). Lou et al. (2016) pointed out that springtime dust concentrations exhibited
74 a significant negative correlation with the East Asian Monsoon Index over most of
75 China with a correlation coefficient of -0.64 in their model simulations, and they found
76 that anomalous northwesterly winds in weak East Asian monsoon years led to a strong
77 dust transport from Mongolia to China. Mao et al. (2011) illustrated that the negative
78 (positive) phase of Arctic Oscillation (AO) can lead to an increase (decrease) in the
79 frequency of dust storms in northern China due to the increase (decrease) in the
80 frequency of cold air outbreak over Mongolia.

81 El Niño-Southern Oscillation (ENSO) is a well-known mode of climate variability

82 generated by coupled ocean-atmosphere interactions that can exert a far-reaching
83 impact on global climate despite its origin in the tropical Pacific Ocean (Trenberth,
84 1997; Yang et al., 2016a, 2016b; Zeng et al., 2021). Numerous studies have
85 demonstrated that El Niño can affect dust emission, concentration and transport by
86 modulating large-scale atmospheric circulation, precipitation and temperature (Le and
87 Bae, 2022; Lee et al., 2015; Li et al., 2021). Using observational data over 1961–2002,
88 Lee et al. (2015) found that under the negative AO phase, frequency of spring dust
89 events in northern China during El Niño was 30% higher than that during La Niña years.
90 Li et al. (2021) used dust surface concentration data (1982–2019) from MERRA-2
91 reanalysis to study the impacts of ENSO events on global atmospheric dust loading and
92 found that dust concentrations were positively correlated with Southern Oscillation
93 Index (SOI, a consistently negative SOI is El Niño and the opposite is La Niña) over
94 northwestern China, which suggests that El Niño was associated with a decrease in dust
95 concentrations. Modeling studies driven by reanalysis data also revealed a relatively
96 weak positive relationship between SOI and dust emissions over Gobi Desert, although
97 this correlation has a large spatiotemporal variation (Gong et al., 2006; Hara et al., 2006).
98 These numerical studies used regional models driven by or nudged to reanalysis
99 meteorological fields, which could be influenced by factors other than El Niño. Recent
100 studies have indicated that the El Niño impact on air pollutants can be better represented
101 by the superposed SST perturbation method (Yu et al., 2019; Zhao et al., 2018; Zeng et
102 al., 2021), considering the influence of ENSO alone. To the best of our knowledge, no
103 study has yet used this approach to investigate the relationship between El Niño and
104 dust pollution in China.

105 Additionally, previous studies mainly focused on the influences of general El Niño
106 on dust over China, while El Niño can be classified into different temporal types (e.g.,
107 short duration (SD) and long duration (LD) El Niño; Guo and Tan, 2018) and spatial
108 types (e.g., East Pacific (EP) and Central Pacific (CP) El Niño; Kao and Yu, 2009).
109 During different spatial and temporal types of El Niño, patterns of precipitation and
110 atmospheric circulation are also different in China (Yu et al., 2019; Zeng et al., 2021),
111 and they could have distinct effects on wintertime and springtime dust pollution in
112 China. Nevertheless, most of the existing studies have focused on the effects of various
113 spatial and temporal types of El Niño events on anthropogenic aerosols, while few
114 studies have examined their effects on natural aerosols, such as dust, and their
115 associated mechanisms, which are crucial for predicting and combating dust pollution

116 in the near future.

117 In this work, the effects of different spatial and temporal types of El Niño on boreal
118 winter and spring dust pollution in China and the mechanisms behind the impacts are
119 examined using the Energy Exascale Earth System Model version 1 (E3SMv1). The
120 methods and model description are described in Section 2. The quantitative impacts of
121 various temporal and spatial types of El Niño events on wintertime and springtime dust
122 concentrations in China and the associated mechanisms are elaborated in Section 3.
123 Section 4 summarizes the key results and conclusions of the study.

124

125 **2. Data and Methods**

126 **2.1 Data**

127 Global SST patterns and SST anomalies during El Niño events of different
128 temporal and spatial types are constructed using the merged Hadley-NOAA/OI dataset
129 which has a horizontal resolution of $1^\circ \times 1^\circ$ from 1870 to 2017 (Hurrell et al., 2008).
130 The monthly ERA5 reanalysis data (Hersbach et al., 2020) are applied to evaluate the
131 simulated meteorological parameters during El Niño events.

132 Hourly observations of PM_{10} (particulate matter less than $10 \mu m$ in diameter)
133 concentrations in China from 2015 to 2021 derived from the China National
134 Environmental monitoring Centre (CNEMC) and the Deep Blue aerosol products
135 (Platnick et al., 2015) from Moderate Resolution Imaging Spectroradiometer (MODIS)
136 on Terra satellite, including monthly Aerosol Optical Depth (AOD) at 550 nm and the
137 Ångström exponent (α) from 2001–2020, are applied to evaluate the performance of
138 dust simulation in the model. The satellite dust optical depth (DOD) is calculated
139 following Yu et al. (2021).

140 **2.2 El Niño events identified as different spatial and temporal types**

141 We first clarify the definition of different temporal and spatial types of El Niño
142 events here. The notation of $year^0$ is used to denote the first year of El Niño
143 development, and Jan^0 , Feb^0 , ..., and Dec^0 indicate the individual months of that year,
144 while $year^{1,2,\dots}$ and $Jan^{1,2,\dots}$, $Feb^{1,2,\dots}$, ..., and $Dec^{1,2,\dots}$, respectively, denote the
145 following years and months therein. Niño 3.4 index is defined as area-mean anomalies
146 of detrended SST in the Niño 3.4 region ($170^\circ W$ – $120^\circ W$, $5^\circ S$ – $5^\circ N$). Niño 3/4 index
147 ($I_{Ni\tilde{a}o3}/I_{Ni\tilde{a}o4}$) is same as Niño 3.4 index, but in the Niño 3/4 region ($150^\circ W$ – $90^\circ W$, $5^\circ S$ –
148 $5^\circ N$; $160^\circ E$ – $150^\circ W$, $5^\circ S$ – $5^\circ N$).

149 For the classification of different temporal types, following Wu et al. (2019), El
 150 Niño events are firstly selected if any of 3-month running averaged Niño 3.4 index
 151 during Oct⁰–Feb¹ greater than 0.75°C. Then the LD El Niño event is identified once
 152 any of Niño 3.4 index during Oct¹–Feb² is higher than 0.5°C; otherwise, it is a SD El
 153 Niño event.

154 Following Yu et al. (2019), the El Niño events, selected with 3-month running
 155 averaged Niño 3.4 indices higher than 0.5°C for five consecutive months, are classified
 156 into different spatial types based on the EP El Niño index (I_{EP}) and the CP El Niño index
 157 (I_{CP}). The definition of these indices is given below.

$$158 \quad I_{EP} = I_{Niño3} - \alpha \times I_{Niño4} \quad (1)$$

$$159 \quad I_{CP} = I_{Niño4} - \alpha \times I_{Niño3} \quad (2)$$

$$160 \quad \alpha = \begin{cases} 0.4, & I_{Niño3} \times I_{Niño4} > 0 \\ 0, & I_{Niño3} \times I_{Niño4} \leq 0 \end{cases} \quad (3)$$

161 If the mean I_{EP} is greater than the I_{CP} during Oct⁰–Feb¹ of an El Niño, then it is an
 162 EP El Niño event; else, it is a CP El Niño event. Note that there also exist mixed El
 163 Niño events that are not considered separately in this study.

164 The time series of Niño 3.4 index derived from Hadley-NOAA/OI 1870–2017 data
 165 is shown in Figure S1. Using the definitions described above, for El Niño with different
 166 temporal types, 22 SD El Niño events and 8 LD ones are extracted during this time
 167 period; for El Niño with different spatial types, 26 EP El Niño events and 8 CP ones are
 168 extracted. The mechanisms leading to different types of El Niño are given in Text S1.

169 **2.3 Model description and experimental design**

170 To investigate the impacts of El Niño of different spatial and temporal types on
 171 dust aerosol in China, this study utilizes the U.S. Department of Energy (DOE)
 172 E3SMv1 (Golaz et al., 2019). As a model developed from the well-known CESM1
 173 (Community Earth System Model version 1), E3SMv1 provides significant
 174 improvements to the atmospheric component, including processes associated with
 175 aerosol, cloud, turbulence, and chemistry (Rasch et al., 2019). We choose the horizontal
 176 resolution of about 1° and 30 vertical layers. E3SMv1 predicts aerosols including
 177 mineral dust, sea salt, sulfate, primary and secondary organic aerosols, and black carbon
 178 in the four-mode Modal Aerosol Module (MAM4) (Wang et al., 2020). E3SMv1
 179 represents dust-related processes in the atmosphere and land model components (Feng
 180 et al., 2022). Dust emissions are calculated at each model time step according to the
 181 wind erosion dust scheme proposed by Zender et al. (2003), which is related to 10-

182 meter wind speed, surface soil moisture content, soil erodibility, vegetation cover and
183 threshold friction velocity.

184 The following simulations are performed. A “CLIM” experiment applying the
185 prescribed climatological mean of monthly SST during 1870–2017 is integrated for 30
186 years. Four sets of sensitivity simulations, “SD”, “LD”, “EP” and “CP”, are driven by
187 the monthly SST representing the composite of SD, LD, EP and CP El Niño events,
188 respectively, which is generated through adding the mean monthly SST anomalies from
189 Jul⁰ to Jun¹ of the SD, LD, EP, and CP El Niño events (Fig. S1), respectively, to the
190 climatological SST between 60°S and 60°N. All the sensitivity experiments have 3
191 ensemble members with diverse initial conditions branched from different years of the
192 CLIM simulation and the results are based on the ensemble mean. All sensitivity
193 experiments are run for 13 years with the first 3 years as model spin-up and the last 10
194 years used for analysis. The differences of model fields between the sensitivity
195 simulations and CLIM represent the influences of El Niño events with different spatial
196 and temporal types on dust aerosols. All other external factors such as greenhouse gas
197 concentrations, insolation, anthropogenic aerosols and their precursor emissions are
198 hold at present-day conditions (year 2014). The SST anomalies relative to the 1870–
199 2017 climatology during SD, LD, EP and CP El Niño events are shown in Fig. 1.

200 **2.4 Model evaluation**

201 To evaluate the model performance in dust simulation, we compare the simulated
202 near-surface dust concentration and dust optical depth (DOD) over China with observed
203 PM₁₀ concentrations and satellite retrieved DOD, respectively. The model can
204 reproduce the spatial distribution of springtime dust in China, with high dust
205 concentrations in northwestern China and low in southern and northeastern China (Fig.
206 S2). The spatial correlation coefficient between the simulated dust concentrations in
207 E3SMv1 and observed near-surface PM₁₀ concentrations is +0.55. However, the model
208 strongly overestimates dust concentrations over the source regions, which were also
209 reported in many previous studies using the E3SMv1 and CESM (the predecessor of
210 E3SMv1) (Wang et al., 2020; Wu et al., 2019). The high model bias near the sources is
211 also confirmed by comparing DOD between model simulation and satellite retrieval. It
212 suggests that the dust emissions are overestimated in northwestern China in the model.
213 The high bias is partly related to the dust treatment in the model that dust is emitted
214 into a shallow model bottom layer in E3SMv1 for increased model vertical resolution
215 (Wang et al., 2020). In addition, stronger 10-m wind speed simulated by the model

216 compared to the observation (Fig. S3) also contributes to the higher dust loading.
217 However, we also note that the E3SMv1 underestimates the transport of dust from
218 source regions (Wu et al., 2020; Feng et al, 2022), thus the dust over eastern China is
219 comparable to observations.

220 **3. Results**

221 **3.1 Impacts of different El Niño types on winter dust pollution**

222 The simulated effects of the four types of El Niño with different spatial positions
223 (EP and CP) and durations (SD and LD) on the DJF ground-level dust concentrations
224 are shown in Fig. 2. As for different spatial types of El Niño events, the effects on DJF
225 dust concentrations in China are similar, with an increase in dust concentrations of 5–
226 50 $\mu\text{g m}^{-3}$ over central-eastern China during EP and CP El Niño compared to the
227 climatological means. The spatial pattern of dust changes is consistent with previous
228 modeling studies (Lee et al., 2015; Li et al., 2021). Although the influences of EP and
229 CP El Niño on the DJF dust concentrations resemble each other in the spatial patterns
230 over China, the magnitudes of the influences are different. During CP El Niño relative
231 to the climatological mean, dust concentrations increase more significantly over
232 central-eastern China, with the increases of 20–50 $\mu\text{g m}^{-3}$, 5–20 $\mu\text{g m}^{-3}$ higher than that
233 during EP El Niño relative to the climatological mean. The large increase during CP El
234 Niño relative to the climatological mean is also more widespread than that during EP
235 El Niño relative to the climatological mean. Compared to CP El Niño, dust
236 concentration over central-eastern China decreased slightly during the EP El Niño, but
237 the changes are mostly insignificant.

238 As for different temporal types of El Niño events, their effects on DJF dust
239 concentrations over China are quite different. SD El Niño events cause an increase in
240 DJF near-surface dust concentrations of 20–100 $\mu\text{g m}^{-3}$ in northern China and about 5–
241 20 $\mu\text{g m}^{-3}$ in southern China. Whereas during LD El Niño events, winter dust
242 concentrations have a decrease of about 5–50 $\mu\text{g m}^{-3}$ in northern and northeastern China
243 relative to the climatology and no significant change is shown in southern China. In
244 contrast to LD El Niño events, SD El Niño events have positive DJF dust concentration
245 anomalies of 5–20 $\mu\text{g m}^{-3}$ in southern China and a maximum over 100 $\mu\text{g m}^{-3}$ in
246 northern China and the Gobi Desert. Furthermore, DJF dust concentrations over the
247 Taklamakan Desert, one of the largest dust sources in China, have an increase during
248 LD El Niño events and an insignificant decrease during SD El Niño events.

249 Overall, these changes in dust concentrations indicate that CP El Niño events have
250 stronger and more widespread impacts on DJF dust concentrations than EP El Niño
251 relative to the climatological mean, and the SD and LD El Niño events exert opposite
252 impacts on DJF dust in China.

253 **3.2 Mechanisms of the different El Niño impacts on winter dust**

254 Meteorological factors such as 10-m wind speed, relative humidity and
255 atmospheric circulation play a dominant role in altering dust concentrations by altering
256 emissions, atmospheric transport, and wet scavenging of dust (Csavina et al., 2014).
257 Dust changes are also controlled by the El Niño-related changes in atmospheric
258 circulation and precipitation (Gong et al., 2006; Hara et al., 2006). The 10-m wind speed,
259 atmospheric circulation, relative humidity, precipitation anomalies, and related
260 processes during EP, CP, SD and LD El Niño are investigated here to reveal the
261 mechanisms of the influence of the four types of El Niño on dust over China.

262 During the CP, EP, and SD El Niño, DJF mean 10-m wind speed increases in the
263 Gobi Desert and northwestern China compared to the climatological mean (Fig. 3),
264 which favors the local dust emission over these regions. Whereas for the LD El Niño
265 event, the positive 10-m wind speed anomaly is greatly weakened, compared to the
266 other three types of El Niño events, and negative 10-m wind speed anomalies are
267 triggered in the Gobi Desert and northern China (Fig. 3e), which is not conducive to
268 dust emission during the LD El Niño events. The CP El Niño events trigger stronger
269 positive 10-m wind speed anomalies ($0.1\text{--}0.3\text{ m s}^{-1}$) than the EP El Niño events over
270 the Gobi Desert and northern China (Fig. 3c), which could lead to a greater local dust
271 emission. Compare to the LD El Niño, SD El Niño events produce significant positive
272 10-m wind speed anomalies of approximately 0.3 m s^{-1} in the Gobi Desert and northern
273 China (Fig. 3f), which is consistent with the increase/decrease in local DJF dust
274 concentrations during the SD/LD El Niño (Fig. 2). This suggests the importance of 10-
275 m wind speed in the dust changes during the El Niño events in China.

276 Figure 4 shows the atmospheric circulation anomalies for the four El Niño events.
277 All types of El Niño have negative anomalies of sea level pressure (SLP) in central-
278 eastern China, except the LD El Niño that shows a negligible SLP change in winter.
279 Meanwhile, during the EP, CP, and SD El Niño events, anomalous Mongolian cyclone
280 can strengthen the local ascending flow to lift more dust particles into the free
281 atmosphere. The anomalous northwesterly during CP and SD El Niño (Figs. 3b and 3d)
282 can transport these dust aerosols to central-eastern China, leading to the strong increases

283 in dust concentrations there (Figs. 2b and 2d). While during the LD El Niño, the lower
284 atmosphere in the Gobi Desert and northern China is controlled by a weak anomalous
285 high pressure accompanied by anomalous southeasterly that weakens the prevailing
286 northwesterly in winter and hinders the vertical lifting and southward transport of dust.

287 Our previous work has confirmed the ability of E3SM in ~~reproducing~~ capturing
288 the atmospheric circulation over central-eastern China in El Niño with different
289 durations (Zeng et al, 2021). Here we further evaluate the circulations in E3SM
290 simulations during EP and CP El Niño events by using ERA5 reanalysis data. The
291 anomalous DJF mean 10-m wind speed and 850 hPa wind fields in the typical EP El
292 Niño (2006/07) and CP El Niño (2014/15) relative to the climatology (1950–2017) from
293 ERA5 are presented in Fig. 5. Although the increase in 10-m wind speed over
294 northwestern China in the EP El Niño simulated in the model is inconsistent with the
295 ERA5 results, E3SM does capture the large increase in wind speed over the Gobi Desert
296 during the CP El Niño relative to the climatological mean and EP El Niño. Moreover,
297 the anomalies in wind fields during EP and CP El Niño (i.e., anomalous southerly
298 during EP El Niño and anomalous northwesterly during CP El Niño ~~are well~~
299 reproduced can be simulated by E3SM. It suggests that the atmospheric circulation
300 features over central-eastern China during different types of El Niño are roughly
301 captured by the model. However, we note that there are notably differences in
302 atmospheric circulation over many regions of East Asia. It can be partly attributed to
303 the model bias in reproducing the atmospheric responses to El Niño. The observations
304 can also be induced by other climate factors besides El Niño, leading to a potential
305 inconsistency in El Niño impact between model and observation.

306 The effect of relative humidity (RH) on dust concentration is also essential,
307 considering that a decrease in RH leads to a decrease in the threshold friction velocity
308 at high RHs (>40%), which further enhances dust emission flux and atmospheric
309 concentration (Csavina et al., 2014). Both EP and CP El Niño events have negative
310 anomalies in DJF RH in the Gobi Desert (Figs. 6a and 6b). The decrease in RH reduces
311 the dust threshold friction velocity and favors dust emission from the Gobi Desert. The
312 CP El Niño produces more pronounced and widespread negative RH anomalies in the
313 Gobi Desert and northwestern China than the EP El Niño. It gives approximately 3%
314 stronger negative RH anomalies (Fig. 6c), resulting in stronger and more widespread
315 increases in DJF dust concentrations during the CP El Niño event (Fig. 2c). As for El
316 Niño with different duration, the SD El Niño leads to significant decreases in DJF RH

317 of about 3% near the south part of the Gobi Desert, while increases in RH are located
318 over north part of the Gobi Desert during the LD El Niño (Figs. 6g and 6j), likely
319 resulting in the opposite changes in dust emissions. The ERA5 reanalysis data also
320 show the same RH variations during the different spatial and temporal types of El Niño
321 as the E3SM simulations described above (Fig. S4). Among all four types of El Niño
322 events, RH anomalies are consistent with the distribution of dust concentration
323 anomalies, which indicates that RH plays an important role in affecting variations in
324 dust emissions and concentrations in China during El Niño.

325 Fig. 7 shows the simulated changes in DJF dust emissions during different El Niño
326 events. During the EP and CP El Niño, DJF dust emissions are enhanced in the Gobi
327 Desert and northwestern China relative to the climatological average. The dust emission
328 increase is larger during the CP El Niño than the EP El Niño, which is consistent with
329 the higher positive DJF dust concentration anomalies during the CP El Niño.
330 Furthermore, the SD El Niño causes a significant increase in dust emissions of about
331 $0.5 \text{ g m}^{-2} \text{ d}^{-1}$ in the Gobi Desert compared to CLIM, while the LD El Niño causes a
332 decrease in dust emissions. These suggest that different types of El Niño events alter
333 the DJF dust emissions in China by changing the 10-m wind speed and RH, which is
334 the important cause of the variation in DJF dust concentrations in China.

335 Furthermore, a reduced DJF precipitation during both EP and CP El Niño events
336 (Fig. S5) should weaken the wet removal of dust from the atmosphere in northern China.
337 However, only insignificant decreases in wet deposition appear in part of northern
338 China and significant increases in wet deposition are located in central and southern
339 China related to increases in dust loading during EP and CP El Niño events (Fig. S6).
340 It suggests that El Niño impact on dust concentrations is mainly through changing the
341 emission and transport of dust rather than the scavenging in winter.

342 **3.3 Spring dust pollution affected by El Niño events**

343 The changes in near-surface dust concentrations over China in the following spring
344 during the decaying phase for different spatial and temporal types of El Niño are also
345 examined (Fig. 8). During the following spring, all El Niño events trigger large positive
346 anomalies of March-April-May (MAM) dust concentrations in northern China.
347 However, the increases in dust concentrations during the EP, CP and SD El Niño relative
348 to the climatological average fail the 90% significance test, indicating that the effects
349 of these types of El Niño events on the dust pollution in northern China in the following
350 spring are uncertain, likely related to the large internal variability of the climate system.

351 In contrast to the strong reduction in dust concentrations over the Gobi Desert and
352 northern China during the LD El Niño in DJF, the effect in MAM reverses to a
353 significant increase in dust concentrations over these regions by 50–100 $\mu\text{g m}^{-3}$ (Fig.
354 8e). It suggests that the weaker intensity but longer duration of LD El Niño than the SD
355 El Niño can significantly affect spring dust aerosols in China.

356 During LD El Niño events, MAM 10-m wind speed significantly increases over
357 the Gobi Desert (Fig. S7), which facilitates the local dust emissions, although RH only
358 shows an insignificant decrease over the dust source region (Fig. S8). It can be
359 confirmed by the significant increases in MAM dust emissions by about 0.5 $\text{g m}^{-2} \text{d}^{-1}$
360 over the Gobi Desert and northwestern China during LD El Niño events (Fig. 9). Then
361 the strengthened northwesterly brings more dust to northern China during LD El Niño
362 events (Fig. S9). Along the transport pathway, the weakened precipitation (Fig. S10)
363 partly reduces the dust wet removal (Fig. S11), leading to the strong increase in MAM
364 dust concentration over northern China during the LD El Niño. However, this effect is
365 largely overwhelmed by the increased dust wet removal due to the emission-induced
366 increase in dust concentrations.

367

368 **4. Conclusion and discussions**

369 Dust, as an important air pollutant affecting air quality in China in winter and
370 spring, can be modulated by the interannual variations in El Niño-induced atmospheric
371 circulation and precipitation anomalies. In this study, the state-of-the-art E3SM model
372 is used to simulate the effects of different temporal types of El Niño events with short
373 (SD) and long duration (LD) and different spatial locations of El Niño events with sea
374 surface temperature anomalies located in Central Pacific (CP) and Eastern Pacific (EP)
375 on dust concentrations in China.

376 Both CP and EP El Niño events cause 5–50 $\mu\text{g m}^{-3}$ positive anomalies in winter
377 (DJF months) surface dust concentrations in central-eastern China. Compared to the EP
378 El Niño, the CP El Niño triggers a stronger wind and negative RH anomalies that lead
379 to greater local dust emissions. Then the anomalous northwesterly transports the dust
380 aerosols to central-eastern China during the CP El Niño, resulting in 5–20 $\mu\text{g m}^{-3}$ higher
381 and more widespread DJF dust concentration increases in northern China, although the
382 changes are mostly statistically insignificant. For the different temporal types of El
383 Niño events, wind speed significantly increases over the Gobi Desert and northern

384 China during the SD El Niño, favoring dust emissions. Meanwhile, the anomalous
385 northwesterly can increase the transport of dust aerosols to central-eastern China,
386 leading to an increase in DJF near-surface dust concentrations of 20–100 $\mu\text{g m}^{-3}$ in
387 northern China and 5–20 $\mu\text{g m}^{-3}$ in southern China relative to the climatological mean.
388 On the contrary, the LD El Niño reduces wind speed over the Gobi Desert and northern
389 China, which weakens dust emissions, accompanied with the atmospheric circulation
390 anomalies unfavorable for dust transport, leading to the DJF dust concentration
391 decrease by 5–50 $\mu\text{g m}^{-3}$ in northern and northeastern China relative to the
392 climatological mean.

393 In the following spring season, the four types of El Niño events with different
394 durations and spatial positions all cause positive dust concentration anomalies in
395 northern China. However, only the changes during the LD El Niño are statistically
396 significant. This is mainly due to an increase in 10-m wind speed over the Gobi Desert
397 during the LD El Niño, which enhances the local dust emissions, and then the
398 strengthened northwesterly brings more dust to the northern China. It suggests that the
399 weaker intensity but longer duration of LD El Niño events than SD El Niño can
400 significantly affect dust aerosols in China in spring.

401 The mechanisms for the differences of the atmospheric anomalies between
402 different types of El Niño have been illustrated in many studies. Western North Pacific
403 anomalous anticyclones (WNPAC), which occur during both EP and CP El Niño events,
404 have been proved as a crucial system that links El Niño and East Asian climate (Li et
405 al., 2017). The anomalous southwesterlies at the north of WNPAC transport moisture
406 to southern China, which can block the prevailing northerlies over central-eastern China
407 in winter and weaken the East Asian winter monsoon (Yuan and Yang, 2012). EP El
408 Niño exerts larger meteorological changes over southern China than CP El Niño due to
409 a stronger WNPAC (Jiang and Li, 2022; Kim et al., 2021). Therefore, the anomalous
410 northerlies over the Gobi Desert and central China are hindered and weaker during EP
411 El Niño than CP El Niño (Fig. 4). SD El Niño has a relatively deeper thermocline during
412 its mature phase than LD El Niño and numerous ocean heat can be transported from the
413 eastern Pacific to the South China Sea and the Western Philippine Sea during SD El
414 Niño (Guo and Tan, 2018). The transmitted ocean heat leads to anomalous warming of
415 the North Pacific SST, a smaller-than-normal tilt of the East Asian trough, a weakening
416 of the mid-latitude westerly flow in front of the trough, and anomalous northerly winds
417 along the trough line of the subtropical trough, along with reduced precipitation (Wang

418 [et al., 2009](#)). [These favor dust emission and transport from north to south during SD El](#)
419 [Niño](#).

420 In this study, the dust concentrations are evaluated by comparing modeled
421 concentrations with MAM PM₁₀ concentrations and the dust loading is also evaluated
422 by comparing modeled DOD with that derived from satellite data. However, the
423 anomalies of dust concentrations were not compared with observations. This is because
424 that dust is jointly influenced by many factors in the observation other than El Niño,
425 such as Mongolian cyclone, sea ice in the Barents Sea, sea surface temperature in
426 Atlantic Ocean, Arctic Oscillation, and human activities (Fan et al 2016, 2018; Mao et
427 al., 2011; Wang et al., 2021; Xiao et al., 2015; Yin et al., 2021), while this study presents
428 the “pure” effects of El Niño on dust using an Earth system model. In addition, PM₁₀ is
429 strongly influenced by other anthropogenic aerosols over eastern China, especially in
430 hazy winter. The comprehensive understanding of the impacts from different types of
431 El Niño events on dust in China requires a longer-term observation with sufficient
432 spatial coverage.

433 Our results contribute to the current knowledge of the vital influence of different
434 types of El Niño on dust pollution in winter and spring over China, which have
435 profound implications for air pollution control and dust storm prediction in China.
436 Notwithstanding, we also note that the E3SMv1 overestimates dust emissions from the
437 source regions and underestimates the long-range transport of dust (Wu et al., 2020;
438 Feng et al, 2022). This high bias of dust loading near the dust source regions are related
439 to the dust treatment in the model, dust parameterization and stronger winds in model
440 than observations. The low bias of long-range transport of dust is due to the strong dust
441 deposition considering that dust is emitted in the shallow model bottom layer in the
442 model. Therefore, the estimate of El Niño impact on dust emissions and concentrations
443 are likely to be overestimated near the source regions, but impact from changes in large-
444 scale circulation related to El Niño on dust transport is possibly underestimated. Also,
445 results from a single model with relative short simulations may not be representative
446 and may not well remove the internal atmospheric variability ([Deser et al., 2014](#)), which
447 can be further investigated by conducting large ensemble and longer simulations using
448 multi-models. In future studies, the influences of different types of La Niña, the cooling
449 phase of ENSO, on dust pollution in China, warrants further investigation. Besides,
450 other natural aerosols, such as sea salt, are also influenced by El Niño events, which is
451 not taken into account in this study. In addition to natural sources, dust in China can

452 also be from anthropogenic emissions (Chen et al., 2019; Xia et al., 2022), and their
453 relations with El Niño require further study.

454 ***Code and data availability***

455 The E3SMv1 model is available at <https://github.com/E3SM-Project/E3SM> (last access:
456 25 Mar 2022) (<http://doi.org/10.11578/E3SM/dc.20180418.36>, E3SM project, 2018).

457 Our results can be made available upon request.

458

459 ***Author contributions***

460 YY designed the research and analyzed the data. LZ performed the model simulations.

461 All the authors including HW, PW, and HL discussed the results and wrote the paper.

462

463 ***Competing interests***

464 The authors declare that they have no conflict of interest.

465

466 ***Acknowledgments***

467 HW acknowledges the support by the U.S. Department of Energy (DOE), Office of
468 Science, Office of Biological and Environmental Research (BER), as part of the Earth
469 and Environmental System Modeling program. The Pacific Northwest National
470 Laboratory (PNNL) is operated for DOE by the Battelle Memorial Institute under
471 contract DE-AC05-76RLO1830.

472

473 ***Financial support***

474 This study was supported by the National Natural Science Foundation of China (grant
475 41975159), the National Key Research and Development Program of China (grant
476 2020YFA0607803 and 2019YFA0606800) and Jiangsu Science Fund for Distinguished
477 Young Scholars (grant BK20211541).

478 **References**

- 479 Chen S. Y., Huang J. P., Li J. X., Jia R., Jiang N. X., Kang L. T., Ma X. J., and Xie T.
480 T.: Comparison of dust emissions, transport, and deposition between the
481 Taklimakan Desert and Gobi Desert from 2007 to 2011. *Sci. China Earth Sci.*, 60,
482 1338–1355, <https://doi.org/10.1007/s11430-016-9051-0>, 2017.
- 483 Chen, S., Zhang, X., Lin, J., Huang, J., Zhao, D., Yuan, T., Huang, K., Luo, Y., Jia, Z.,
484 and Zang, Z.: Fugitive Road Dust PM_{2.5} Emissions and Their Potential Health
485 Impacts, *Environ. Sci. Technol.*, 53, 8455–8465,
486 <https://doi.org/10.1021/acs.est.9b00666>, 2019.
- 487 Csavina, J., Field, J., Felix, O., Corral-Avitia, A. Y., Saez, A. E., and Betterton, E. A.:
488 Effect of wind speed and relative humidity on atmospheric dust concentrations in
489 semi-arid climates, *Sci Total Environ*, 487, 82–90,
490 <https://doi.org/10.1016/j.scitotenv.2014.03.138>, 2014.
- 491 [Deser, C., Phillips, A. S., Alexander, M. A., and Smoliak, B. V., Projecting North](#)
492 [American climate over the next 50 years: uncertainty due to internal variability. *J.*](#)
493 [*Clim.*, 27, 2271–2296, 2014, <https://doi.org/10.1175/JCLI-D-13-00451.1>.](#)
- 494 E3SM Project: Energy Exascale Earth System Model v1.0: Computer Software, DOE
495 [data set], <https://doi.org/10.11578/E3SM/dc.20180418.36>, 2018.
- 496 Fan, K., Xie, Z., and Xu, Z.: Two different periods of high dust weather frequency in
497 northern China, *Atmos. Ocean. Sci. Lett.*, 9, 263–269,
498 <https://doi.org/10.1080/16742834.2016.1176300>, 2016.
- 499 Fan, K., Xie, Z., Wang, H., Xu, Z., and Liu, J.: Frequency of spring dust weather in
500 North China linked to sea ice variability in the Barents Sea, *Clim. Dyn.*, 51, 4439–
501 4450, <https://doi.org/10.1007/s00382-016-3515-7>, 2018.
- 502 Feng, Y., Wang, H., Rasch, P. J., Zhang, K., Lin, W., Tang, Q., Xie, S., Hamilton, D. S.,
503 Mahowald, N., and Yu, H.: Global dust cycle and direct radiative effect in the
504 E3SM version 1: Impact of increasing model resolution, *J. Adv. Model. Earth Sys.*,
505 14, e2021MS002909. <https://doi.org/10.1029/2021MS002909>, 2022.
- 506 Golaz, J. C., Caldwell, P. M., Van Roekel, L. P., Petersen, M. R., Tang, Q., Wolfe, J. D.,
507 Abeshu, G., Anantharaj, V., Asay - Davis, X. S., Bader, D. C., Baldwin, S. A.,
508 Bisht, G., Bogenschutz, P. A., Branstetter, M., Brunke, M. A., Brus, S. R., Burrows,
509 S. M., Cameron - Smith, P. J., Donahue, A. S., Deakin, M., Easter, R. C., Evans,
510 K. J., Feng, Y., Flanner, M., Foucar, J. G., Fyke, J. G., Griffin, B. M., Hannay, C.,

511 Harrop, B. E., Hoffman, M. J., Hunke, E. C., Jacob, R. L., Jacobsen, D. W., Jeffery,
 512 N., Jones, P. W., Keen, N. D., Klein, S. A., Larson, V. E., Leung, L. R., Li, H. Y.,
 513 Lin, W., Lipscomb, W. H., Ma, P. L., Mahajan, S., Maltrud, M. E., Mامتjanov,
 514 A., McClean, J. L., McCoy, R. B., Neale, R. B., Price, S. F., Qian, Y., Rasch, P. J.,
 515 Reeves Eyre, J. E. J., Riley, W. J., Ringler, T. D., Roberts, A. F., Roesler, E. L.,
 516 Salinger, A. G., Shaheen, Z., Shi, X., Singh, B., Tang, J., Taylor, M. A., Thornton,
 517 P. E., Turner, A. K., Veneziani, M., Wan, H., Wang, H., Wang, S., Williams, D. N.,
 518 Wolfram, P. J., Worley, P. H., Xie, S., Yang, Y., Yoon, J. H., Zelinka, M. D., Zender,
 519 C. S., Zeng, X., Zhang, C., Zhang, K., Zhang, Y., Zheng, X., Zhou, T., and Zhu,
 520 Q.: The DOE E3SM Coupled Model Version 1: Overview and Evaluation at
 521 Standard Resolution, *J. Adv. Model. Earth Sys.*, 11, 2089–2129,
 522 <https://doi.org/10.1029/2018MS001603>, 2019.

523 Gong, S. L., Zhang, X. Y., Zhao, T. L., Zhang, X. B., Barrie, L. A., McKendry, I. G.,
 524 and Zhao, C. S.: A Simulated Climatology of Asian Dust Aerosol and Its Trans-
 525 Pacific Transport. Part I: Interannual Variability and Climate, *J. Clim.*, 19, 104–
 526 122, <https://doi.org/10.1175/JCLI3606.1>, 2006.

527 Goudie, A. S.: Desert dust and human health disorders, *Environ. Int.*, 63, 101–113,
 528 <https://doi.org/10.1016/j.envint.2013.10.011>, 2014.

529 Guo, J., Xu, H., Liu, L., Chen, D., Peng, Y., Yim, S. H.-L., Yang, Y., Li, J., Zhao, C.,
 530 and Zhai, P.: The trend reversal of dust aerosol over East Asia and the North Pacific
 531 Ocean attributed to large-scale meteorology, deposition, and soil moisture. *J.*
 532 *Geophys. Res. Atmos.*, 124, 10450–10466.
 533 <https://doi.org/10.1029/2019JD030654>, 2019.

534 Guo, Y., and Tan, Z.: Westward migration of tropical cyclone rapid-intensification over
 535 the Northwestern Pacific during short duration El Nino, *Nat. Commun.*, 9, 1507,
 536 <https://doi.org/10.1038/s41467-018-03945-y>, 2018.

537 Hara, Y., Uno, I., and Wang, Z.: Long-term variation of Asian dust and related climate
 538 factors, *Atmos. Environ.* 40, 6730–6740,
 539 <https://doi.org/10.1016/j.atmosenv.2006.05.080>, 2006.

540 Hersbach, H., Bell, B., Berrisford, P., Hirahara, S., Horányi, A., Muñoz-Sabater, J.,
 541 Nicolas, J., Peubey, C., Radu, R., Schepers, D., Simmons, A., Soci, C., Abdalla,
 542 S., Abellan, X., Balsamo, G., Bechtold, P., Biavati, G., Bidlot, J., Bonavita, M.,
 543 Chiara, G. D., Dahlgren, P., Dee, D., Diamantakis, M., Dragani, R., Flemming, J.,
 544 Forbes, R., Fuentes, M., Geer, A., Haimberger, L., Healy, S., Hogan, R. J., Hólm,

545 E., Janisková, M., Keeley, S., Laloyaux, P., Lopez, P., Lupu, C., Radnoti, G.,
546 Rosnay, P. de, Rozum, I., Vamborg, F., Villaume, S., and Thépaut, J.-N.: The ERA5
547 Global Reanalysis, *Q. J. Roy. Meteor. Soc.*, 146, 1999–2049,
548 <https://doi.org/10.1002/qj.3803>, 2020.

549 Huang, J., Wang, T., Wang, W., Li, Z., and Yan, H.: Climate effects of dust aerosols
550 over East Asian arid and semiarid regions, *J. Geophys. Res. Atmos.*, 119, 11,398–
551 11,416, <https://doi.org/10.1002/2014JD021796>, 2014.

552 Hurrell, J. W., Hack, J. J., Shea, D., Caron, J. M., and Rosinski, J.: A new sea surface
553 temperature and sea ice boundary dataset for the Community Atmosphere Model,
554 *J. Clim.*, 21, 5145–5153, <https://doi.org/10.1175/2008jcli2292.1>, 2008.

555 [Jiang, Z. and Li, J.: Impact of eastern and central Pacific El Niño on lower tropospheric](#)
556 [ozone in China, *Atmos. Chem. Phys.*, 22, 7273–7285, \[https://doi.org/10.5194/acp-\]\(https://doi.org/10.5194/acp-22-7273-2022\)](#)
557 [22-7273-2022, 2022.](#)

558 Kao, H-Y., and Yu, J-Y.: Contrasting Eastern-Pacific and Central-Pacific Types of
559 ENSO, *J. Clim.*, 22, 615–632, <https://doi.org/10.1175/2008jcli2309.1>, 2009.

560 [Kim, J., Chang, T., Lee, C., and Yu, J.: On the Varying Responses of East Asian Winter](#)
561 [Monsoon to Three Types of El Niño: Observations and Model Hindcasts, *J. Clim.*,](#)
562 [34, 4089–4101, <https://doi.org/10.1175/JCLI-D-20-0784.1>, 2021.](#)

563 Kok, J. F., Ward, D. S., Mahowald, N. M., and Evan, A. T.: Global and regional
564 importance of the direct dust-climate feedback. *Nat. Commun.*, 9, 241,
565 <https://doi.org/10.1038/s41467-017-02620-y>, 2018.

566 Le, T. and Bae, D.-H.: Causal influences of El Niño-Southern Oscillation on global dust
567 activities, *Atmos. Chem. Phys.*, 22, 5253-5263, [https://doi.org/10.5194/acp-22-](https://doi.org/10.5194/acp-22-5253-2022)
568 [5253-2022, 2022.](#)

569 Lee, Y. G., Kim, J., Ho, C.-H., An, S.-I., Cho, H.-K., Mao, R., Tian, B., Wu, D., Lee, J.
570 N., Kalashnikova, O., Choi, Y., and Yeh, S.-W.: The effects of ENSO under
571 negative AO phase on spring dust activity over northern China: an observational
572 investigation, *Int. J. Climatol.*, 35, 935–947, <https://doi.org/10.1002/joc.4028>,
573 2015.

574 Li, J., Garshick, E., Al-Hemoud, A., Huang, S., and Koutrakis, P.: Impacts of
575 meteorology and vegetation on surface dust concentrations in Middle Eastern
576 countries, *Sci. Total Environ.*, 712, 136597,
577 <https://doi.org/10.1016/j.scitotenv.2020.136597>, 2020.

578 Li, J., Garshick, E., Huang, S., and Koutrakis, P.: Impacts of El Niño-Southern

579 Oscillation on surface dust levels across the world during 1982–2019, *Sci. Total*
580 *Environ.*, 769, 144566, <https://doi.org/10.1016/j.scitotenv.2020.144566>, 2021.

581 [Li, T., Wang, B., Wu, B., Zhou, T., Chang, C. P., and Zhang, R.: Theories on formation](#)
582 [of an anomalous anticyclone in western North Pacific during El Niño: A review, *J.*](#)
583 [*Meteorol. Res.*, 31, 987–1006, <https://doi.org/10.1007/s13351-017-7147-6>, 2017.](#)

584 Lou, S., Russell, L. M., Yang, Y., Xu, L., Lamjiri, M. A., DeFlorio, M. J., Miller, A. J.,
585 Ghan, S. J., Liu, Y., and Singh, B.: Impacts of the East Asian Monsoon on
586 springtime dust concentrations over China, *J. Geophys. Res. Atmos.*, 121, 813 7–
587 8152, <https://doi.org/10.1002/2016JD024758>, 2016.

588 Mao, R., Gong, D., Bao, J., and Fan, Y.: Possible influence of Arctic Oscillation on dust
589 storm frequency in North China. *J. Geogr. Sci.* 21, 207–218,
590 <https://doi.org/10.1007/s11442-011-0839-4>, 2011.

591 Platnick, S., Hubanks, P., Meyer, K., and King, M. D.: MODIS Atmosphere L3 Monthly
592 Product (08_L3). NASA MODIS Adaptive Processing System, Goddard Space
593 Flight Center, http://dx.doi.org/10.5067/MODIS/MOD08_M3.006, 2015.

594 Rasch, P. J., Xie, S., Ma, P. L., Lin, W., Wang, H., Tang, Q., Burrows, S. M., Caldwell,
595 P., Zhang, K., Easter, R. C., Cameron-Smith, P., Singh, B., Wan, H., Golaz, J. C.,
596 Harrop, B. E., Roesler, E., Bacmeister, J., Larson, V. E., Evans, K. J., Qian, Y.,
597 Taylor, M., Leung, L. R., Zhang, Y., Brent, L., Branstetter, M., Hannay, C.,
598 Mahajan, S., Mаметjanov, A., Neale, R., Richter, J. H., Yoon, J. H., Zender, C. S.,
599 Bader, D., Flanner, M., Foucar, J. G., Jacob, R., Keen, N., Klein, S. A., Liu, X.,
600 Salinger, A. G., Shrivastava, M., and Yang, Y.: An Overview of the Atmospheric
601 Component of the Energy Exascale Earth System Model, *J. Adv. Model Earth Sy.*,
602 11, 2377–2411, <https://doi.org/10.1029/2019MS001629>, 2019.

603 Seinfeld, J. H., Carmichael, G. R., Arimoto, R., Conant, W. C., Brechtel, F. J., Bates, T.
604 S., Cahill, T. A., Clarke, A. D., Doherty, S. J., Flatau, P. J., Huebert, B. J., Kim, J.,
605 Markowicz, K. M., Quinn, P. K., Russell, L. M., Russell, P. B., Shimizu, A.,
606 Shinozuka, Y., Song, C. H., Tang, Y., Uno, I., Vogelmann, A. M., Weber, R. J., Woo,
607 J.-H., and Zhang, X. Y.: ACE-ASIA: Regional Climatic and Atmospheric
608 Chemical Effects of Asian Dust and Pollution, *Bull. Am. Meteorol. Soc.*, 85, 367–
609 380, <https://doi.org/10.1175/BAMS-85-3-367>, 2004.

610 Shi, L., Zhang, J., Yao, F., Zhang, D., and Guo, H.: Drivers to dust emissions over dust
611 belt from 1980 to 2018 and their variation in two global warming phases, *Sci. Total*
612 *Environ.*, 767, 144806, <https://doi.org/10.1016/j.scitotenv.2020.144860>, 2021.

613 Sivakumar M. V.: Impacts of Sand Storms/Dust Storms on Agriculture, in: Natural
614 Disasters and Extreme Events in Agriculture, edited by: Sivakumar M.V., Motha
615 R.P., and Das H.P. Springer, Berlin, Heidelberg, 159–177,
616 https://doi.org/10.1007/3-540-28307-2_10, 2005.

617 Trenberth K. E.: The definition of El Niño, *Bull. Am. Meteorol. Soc.*, 78(12), 2771–
618 2778, [https://doi.org/10.1175/1520-0477\(1997\)078<2771:TDOENO>2.0.CO;2](https://doi.org/10.1175/1520-0477(1997)078<2771:TDOENO>2.0.CO;2),
619 1997.

620 [Wang, L., Chen, W., Zhou, W., and Huang, R.: Interannual Variations of East Asian](#)
621 [Trough Axis at 500 hPa and its Association with the East Asian Winter Monsoon](#)
622 [Pathway, *J. Clim.*, 22, 600–614, <https://doi.org/10.1175/2008JCLI2295.1>, 2009.](#)

623 Wang, H., Easter, R. C., Zhang, R., Ma, P.-L., Singh, B., Zhang, K., Ganguly, D., Rasch,
624 P. J., Burrows, S. M., Ghan, S. J., Lou, S., Qian, Y., Yang, Y., Feng, Y., Flanner,
625 M., Leung, L. R., Liu, X., Shrivastava, M., Sun, J., Tang, Q., Xie, S., and Yoon, J.-
626 H., Aerosols in the E3SM Version 1: New developments and their impacts on
627 radiative forcing, *J. Adv. Model. Earth Sys.*, 12, e2019MS001851,
628 <https://doi.org/10.1029/2019MS001851>, 2020.

629 Wang, S., Yu, Y., Zhang, X., Lu, H., Zhang, X., and Xu, Z.: Weakened dust activity over
630 China and Mongolia from 2001 to 2020 associated with climate change and land-
631 use management, *Environ. Res. Lett.*, 16, 124056, [https://doi.org/10.1088/1748-](https://doi.org/10.1088/1748-9326/ac3b79)
632 [9326/ac3b79](https://doi.org/10.1088/1748-9326/ac3b79), 2021.

633 Wu, M., Liu, X., Yang, K., Luo, T., Wang, Z., Wu, C., Zhang, K., Yu, H., and Darmenov,
634 A.: Modeling Dust in East Asia by CESM and Sources of Biases, *J. Geophys. Res.*
635 *Atmos.*, 124, 8043–8064. <https://doi.org/10.1029/2019JD030799>, 2019.

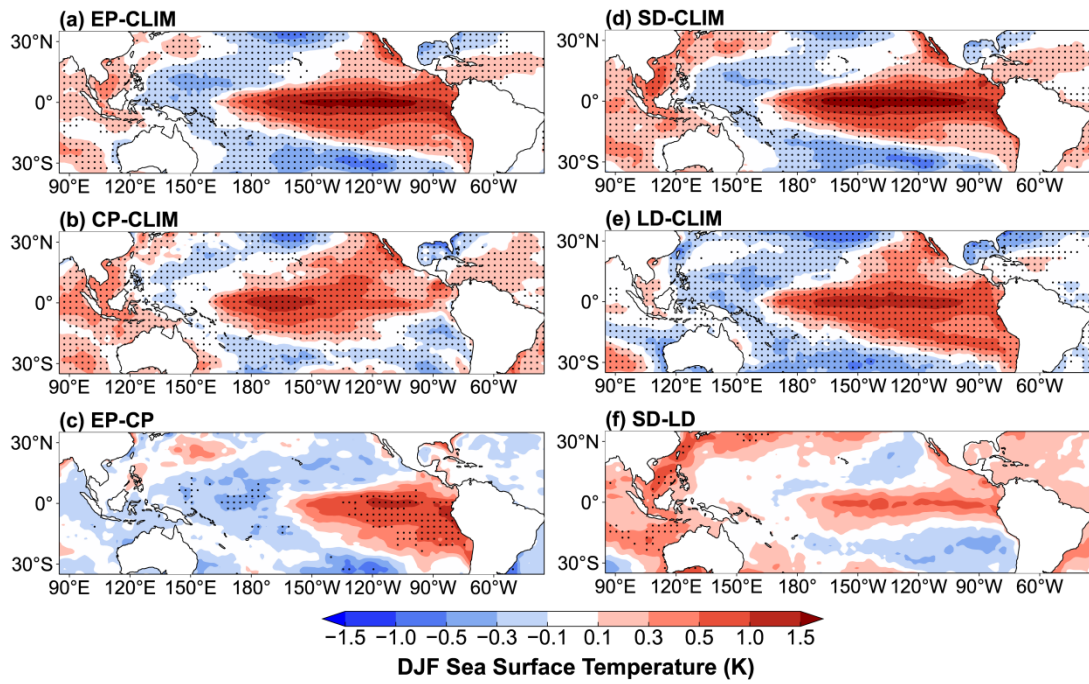
636 Wu, M., Liu, X., Yu, H., Wang, H., Shi, Y., Yang, K., Darmenov, A., Wu, C., Wang, Z.,
637 Luo, T., Feng, Y., and Ke, Z.: Understanding processes that control dust spatial
638 distributions with global climate models and satellite observations, *Atmos. Chem.*
639 *Phys.*, 20, 13835–13855, <https://doi.org/10.5194/acp-20-13835-2020>, 2020.

640 Wu, X., Okumura, Y. M., and Dinezio, P. N.: What Controls the Duration of El Niño
641 and La Niña Events?, *J. Clim.*, 32, 5941–5965, [https://doi.org/10.1175/jcli-d-18-](https://doi.org/10.1175/jcli-d-18-0681.1)
642 [0681.1](https://doi.org/10.1175/jcli-d-18-0681.1), 2019.

643 Xia, W., Wang, Y., Chen, S., Huang, J., Wang, B., Zhang, G. J., Zhang, Y., Liu, X., Ma,
644 J., Gong, P., Jiang, Y., Wu, M., Xue, J., Wei, L., and Zhang, T.: Double Trouble of
645 Air Pollution by Anthropogenic Dust, *Environ. Sci. Technol.*, 56, 761–769,
646 <https://doi.org/10.1021/acs.est.1c04779>, 2022.

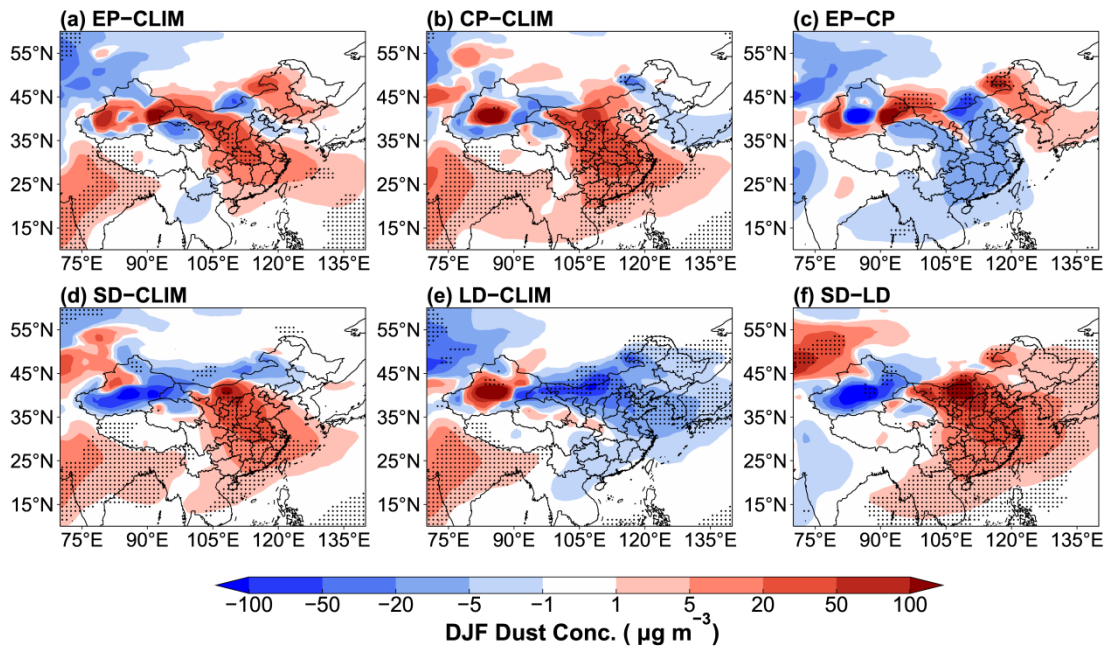
- 647 Xiao, D., Li, Y., Fan, S., Zhang, R., Sun, J., and Wang, Y.: Plausible influence of Atlantic
648 Ocean SST anomalies on winter haze in China, *Theor. Appl. Climatol.*, 122, 249-
649 257, <https://doi.org/10.1007/s00704-014-1297-6>, 2015.
- 650 Yang, Y., Russell, L. M., Xu, L., Lou, S., Lamjiri, M. A., Somerville, R. C. J., Miller,
651 A. J., Cayan, D. R., DeFlorio, M. J., Ghan, S. J., Liu, Y., Singh, B., Wang, H., Yoon,
652 J.-H., and Rasch, P. J.: Impacts of ENSO events on cloud radiative effects in
653 preindustrial conditions: Changes in cloud fraction and their dependence on
654 interactive aerosol emissions and concentrations, *J. Geophys. Res. Atmos.*, 121,
655 6321–6335, <https://doi.org/10.1002/2015jd024503>, 2016a.
- 656 Yang, Y., Russell, L. M., Lou, S., Liu, Y., Singh, B., and Ghan, S. J.: Rain-aerosol
657 relationships influenced by wind speed, *Geophys. Res. Lett.*, 43, 2267–2274,
658 <https://doi.org/10.1002/2016GL067770>, 2016b.
- 659 Yang, Y., Russell, L. M., Lou, S., Liao, H., Guo, J., Liu, Y., Singh, B., and Ghan, S. J.:
660 Dust-wind interactions can intensify aerosol pollution over eastern China, *Nat.*
661 *Commun.*, 8, 15333, <https://doi.org/10.1038/ncomms15333>, 2017.
- 662 Yin, Z., Wan, Y., Zhang, Y., and Wang, H.: Why super sandstorm 2021 in North China?,
663 *Natl. Sci. Rev.*, <https://doi.org/10.1093/nsr/nwab165>, 2021.
- 664 Yu, X., Wang, Z., Zhang, H., and Zhao, S.: Impacts of different types and intensities of
665 El Niño events on winter aerosols over China, *Sci. Total Environ.*, 655, 766–780,
666 <https://doi.org/10.1016/j.scitotenv.2018.11.090>, 2019.
- 667 Yu, Y. and Ginoux, P.: Assessing the contribution of the ENSO and MJO to Australian
668 dust activity based on satellite- and ground-based observations, *Atmos. Chem.*
669 *Phys.*, 21, 8511–8530, <https://doi.org/10.5194/acp-21-8511-2021>, 2021.
- 670 [Yuan, Y., and Yang, S.: Impacts of Different Types of El Niño on the East Asian Climate:
671 Focus on ENSO Cycles, *J. Clim.*, 25, 7702 – 7722, \[https://doi.org/10.1175/JCLI-
D-11-00576.1\]\(https://doi.org/10.1175/JCLI-
672 D-11-00576.1\), 2012.](#)
- 673 Zender, C. S., Bian, H., and Newman, D.: Mineral Dust Entrainment and Deposition
674 (DEAD) model: Description and 1990s dust climatology, *J. Geophys. Res.*, 108,
675 4416, <https://doi.org/10.1029/2002JD002775>, 2003.
- 676 Zeng, L., Yang, Y., Wang, H., Wang, J., Li, J., Ren, L., Li, H., Zhou, Y., Wang, P., and
677 Liao, H.: Intensified modulation of winter aerosol pollution in China by El Niño
678 with short duration, *Atmos. Chem. Phys.*, 21, 10745–10761,
679 <https://doi.org/10.5194/acp-21-10745-2021>, 2021.
- 680 Zhao, S., Zhang, H., and Xie, B.: The effects of El Niño-Southern Oscillation on the

681 winter haze pollution of China, *Atmos. Chem. and Phys.*, 18, 1863–1877,
682 <https://doi.org/10.5194/acp-18-1863-2018>, 2018.
683 Zhu, C., Wang, B., and Qian, W.: Why do dust storms decrease in northern China
684 concurrently with the recent global warming?, *Geophys. Res. Lett.*, 35, L18702,
685 <https://doi.org/10.1029/2008GL034886>, 2008.
686



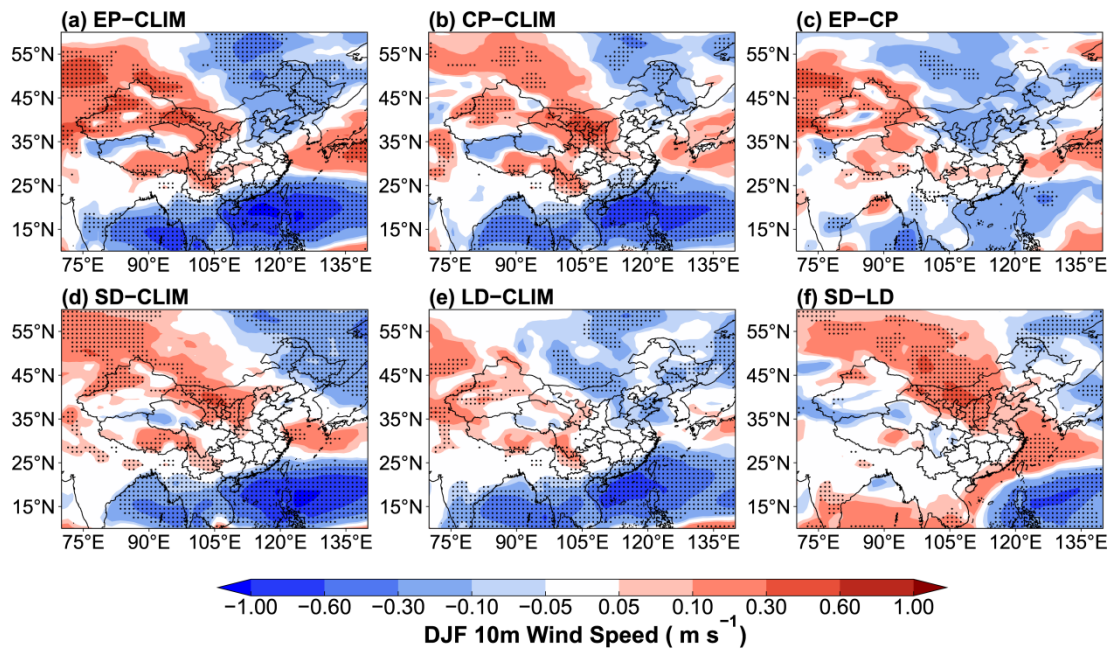
687
 688
 689
 690
 691
 692

Figure 1. Composite differences in DJF mean SST ($^{\circ}\text{C}$) between (a) EP, (b) CP, (d) SD, (e) LD El Niño events and climatological mean over 1870–2017, and (c) between EP and CP, and (f) between SD and LD El Niño events. Statistically significant differences at 99% from a two-tailed T-test are stippled.



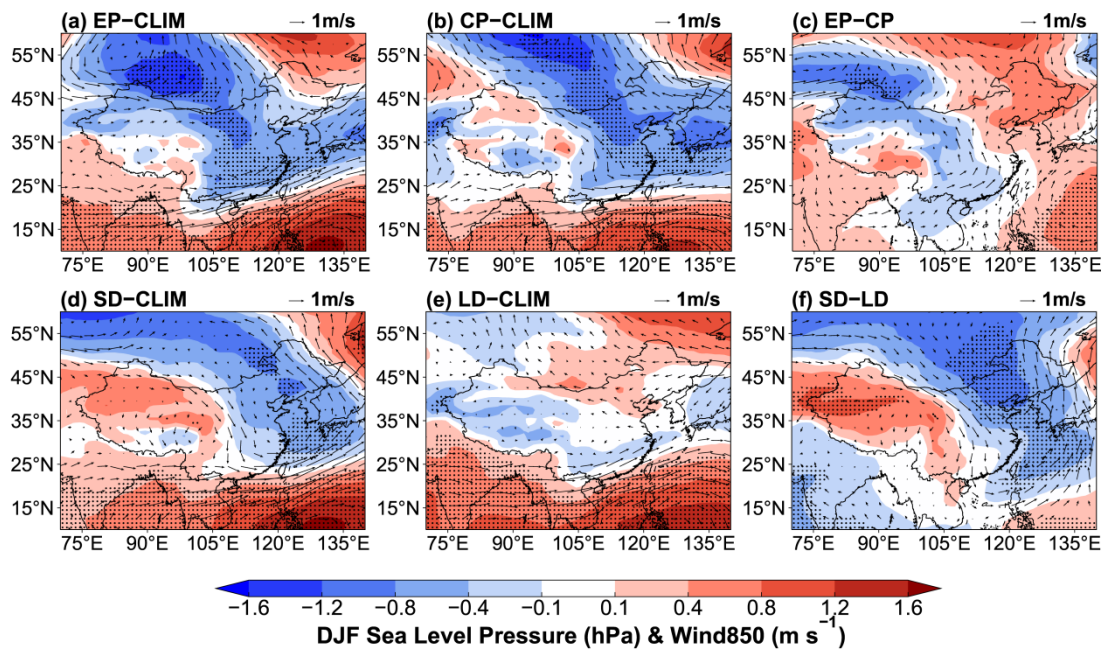
693
 694
 695
 696
 697
 698

Figure 2. Composite differences in DJF mean near-surface dust concentrations ($\mu\text{g m}^{-3}$) between EP and CLIM in (a), CP and CLIM in (b), EP and CP in (c), SD and CLIM in (d), LD and CLIM in (e), and SD and LD in (f). The stippled areas indicate statistical significance with 90% confidence from a two-tailed T-test.



699
 700
 701
 702
 703
 704

Figure 3. Composite differences in DJF mean 10-m wind speed (m s^{-1}) between EP and CLIM in (a), CP and CLIM in (b), EP and CP in (c), SD and CLIM in (d), LD and CLIM in (e), and SD and LD in (f). The stippled areas indicate statistical significance with 90% confidence from a two-tailed T-test.



706

707

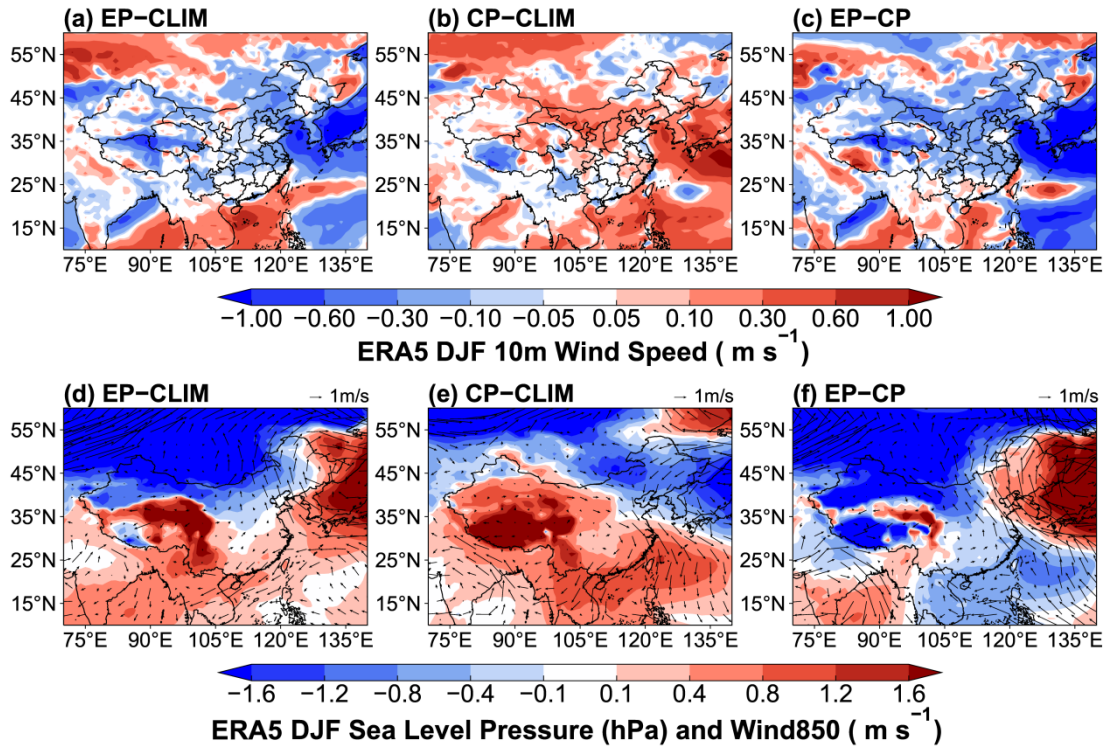
708

709

710

711

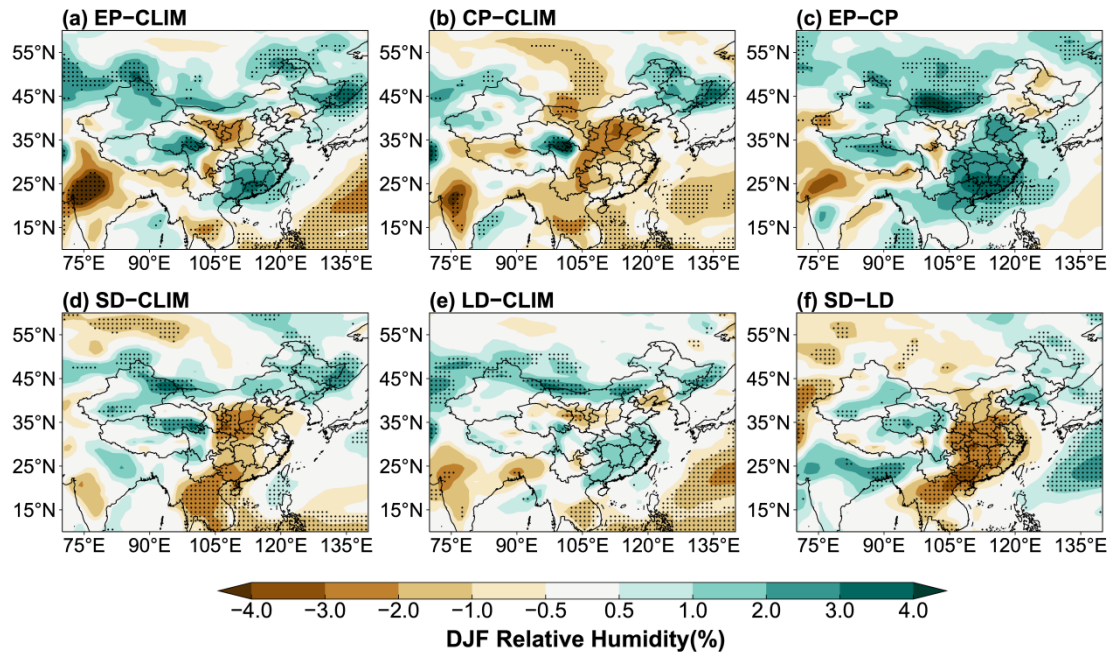
Figure 4. Composite differences in DJF mean sea level pressure (SLP, shaded; units: hPa) and winds at 850 hPa (WIND850, vector; units: m s⁻¹) between EP and CLIM in (a), CP and CLIM in (b), and EP and CP in (c), SD and CLIM in (d), LD and CLIM in (e), and SD and LD in (f). The stippled areas indicate statistical significance with 90% confidence from a two-tailed T-test.



712

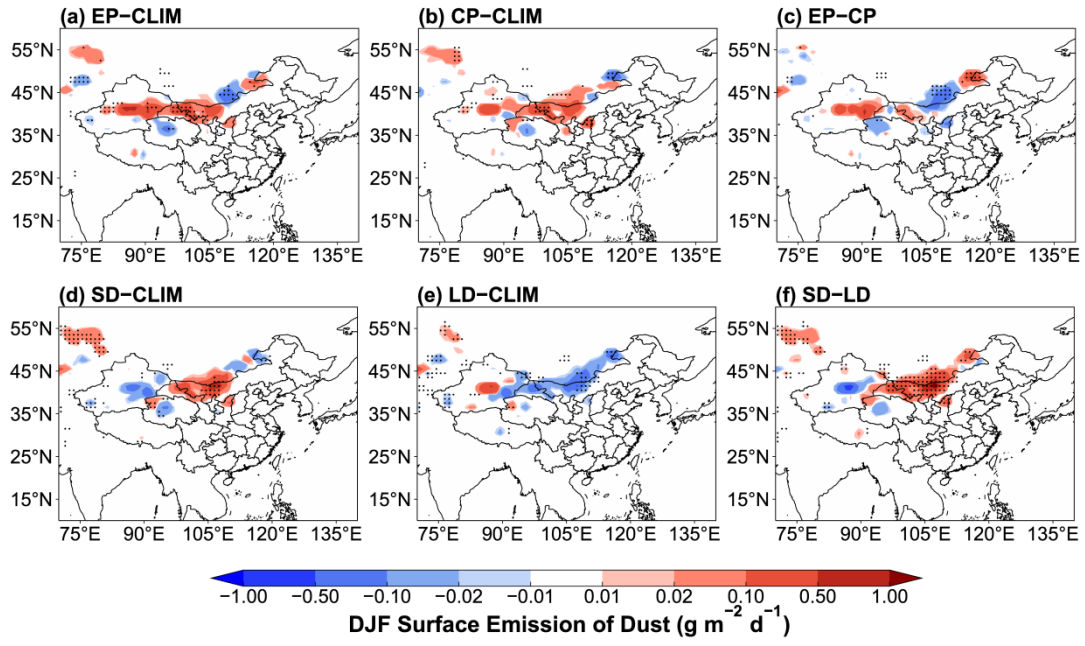
713 **Figure 5.** Composite differences in DJF mean 10-m wind speed (m s^{-1}) (top panels) and sea level
 714 pressure (SLP, shaded; units: hPa) and wind at 850 hPa (WIND850, vector; units: m s^{-1}) (bottom
 715 panels) between 2006/07 EP El Niño and climatological mean (1950–2017) in (a, d), 2014/15 CP
 716 El Niño and climatological mean in (b, e), and 2006/07 EP El Niño and 2014/15 CP El Niño in (c,
 717 f) from the ERA5 reanalysis data. The data were detrended over 1950–2017.

718



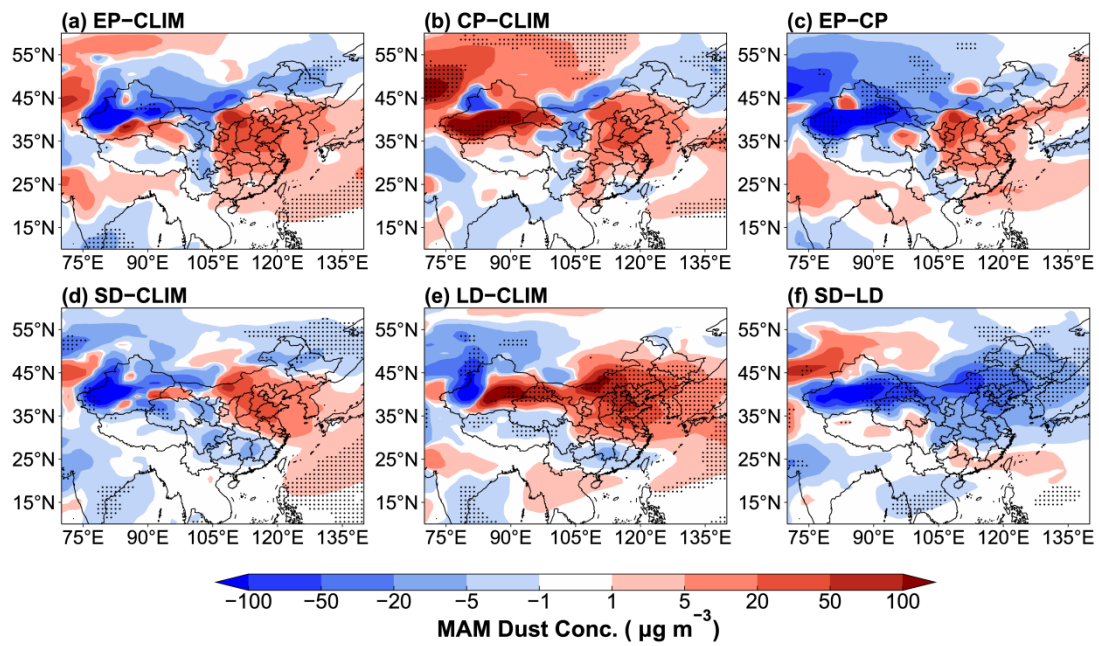
719

720 **Figure 6.** Composite differences in DJF mean relative humidity (units: %) between EP and CLIM
 721 in (a), CP and CLIM in (b), and EP and CP in (c), SD and CLIM in (d), LD and CLIM in (e), and
 722 SD and LD in (f). The stippled areas indicate statistical significance with 90% confidence from a
 723 two-tailed T-test.
 724



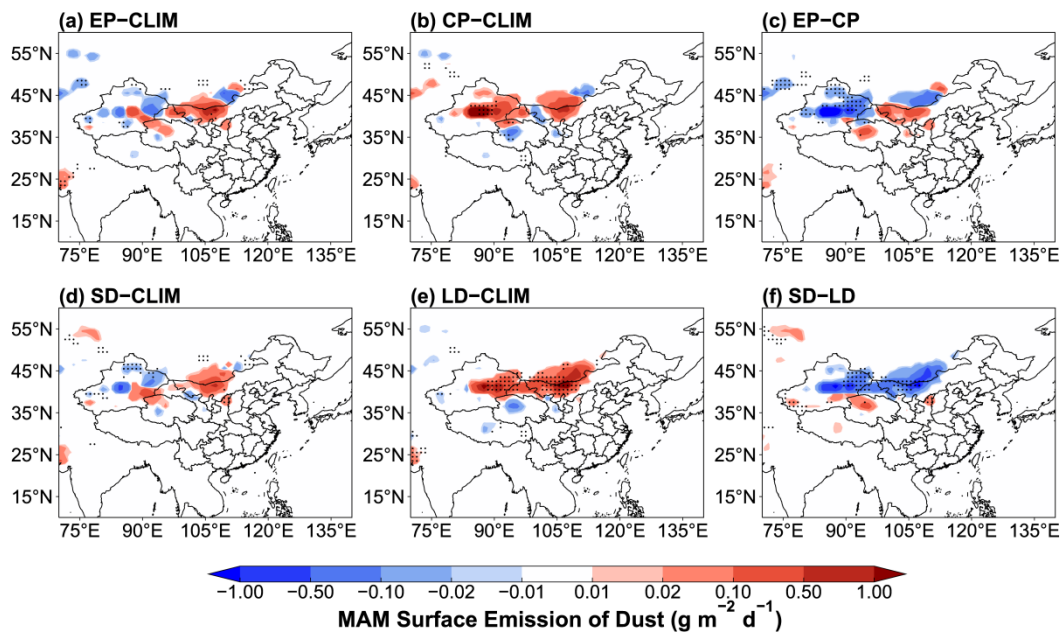
725
 726
 727
 728
 729
 730

Figure 7. Composite differences in DJF mean dust emissions ($\text{g m}^{-2} \text{d}^{-1}$) between EP and CLIM in (a), CP and CLIM in (b), EP and CP in (c), SD and CLIM in (d), LD and CLIM in (e), and SD and LD in (f). The stippled areas indicate statistical significance with 90% confidence from a two-tailed T-test.



731
 732
 733
 734
 735
 736

Figure 8. Composite differences in MAM mean near-surface dust concentrations ($\mu\text{g m}^{-3}$) between EP and CLIM in (a), CP and CLIM in (b), EP and CP in (c), SD and CLIM in (d), LD and CLIM in (e), and SD and LD in (f). The stippled areas indicate statistical significance with 90% confidence from a two-tailed T-test.



738

739

740

741

742

743

Figure 9. Composite differences in MAM mean dust emissions ($\text{g m}^{-2} \text{d}^{-1}$) between EP and CLIM in (a), CP and CLIM in (b), EP and CP in (c), SD and CLIM in (d), LD and CLIM in (e), and SD and LD in (f). The stippled areas indicate statistical significance with 90% confidence from a two-tailed T-test.